PAPER

Check for updates

Microwave-assisted synthesis of a sulfonated carbon-based catalyst for efficient esterification of oleic acid into biodiesel

Michelle P. Duarte, [iD] [ab] Luis Páramo[ab] and Rafik Naccache [iD] *[ab]

Carbon-based solid acid catalysts have emerged as an efficient alternative for the esterification of non-edible oils into biodiesel. However, their preparation often relies on post-synthetic sulfonation with harsh acids or high-energy-demanding methods, such as hydrothermal carbonization. In this work, a sulfonated carbon catalyst derived from sucrose and *p*-toluenesulfonic acid was developed *via* a one-pot hydrothermal microwave-assisted method, in search of a more sustainable and energy-efficient catalyst route. A synthesis study was performed by varying the sucrose : *p*-toluenesulfonic mass ratio (1 : 0.5–1 : 2), temperature (140–220 °C), and reaction time (10–30 min). The synthesis conditions 1 : 1.5 mass ratio, 180 °C, and 20 minutes were selected as optimal as they provided a favourable balance between catalytic activity and energy consumption, achieving 90.2% conversion under preliminary esterification conditions (1 : 9 oleic acid-to-methanol, 90 °C, 3 h, 5 wt% catalyst). Characterization confirmed the successful incorporation of sulfonic groups ($-SO_3H$ density of 0.20 mmol g^{-1}). Esterification parameters were further optimized using a one-variable-at-a-time approach, evaluating the effects of oil-to-methanol molar ratio (1 : 6–1 : 30), catalyst loading (1–7 wt%), temperature (70–90 °C), and time (0.5–5 h). Under optimal conditions (1 : 18 molar ratio, 5 wt%, 90 °C, 30 min), a conversion of 91% was achieved, demonstrating strong performance at short reaction times. Reusability tests showed a significant drop in performance after the second cycle, likely due to the leaching of active sites. However, the catalyst's low cost, fast synthesis, and strong performance under mild conditions render it a valuable option for more sustainable biodiesel production.

Introduction

Energy insecurity, pollution, climate change, and the rise in fossil fuel costs are some of the challenges the world has faced in recent decades.[1,2] As a result, the United Nations (UN) has established 17 Sustainable Development Goals (SDGs) in order to address these issues and promote a sustainable future. As the need to protect the environment has become more crucial, six of these goals are directly related to environmental protection, with efforts focused on sectors such as energy, industry, and transportation.[1,3] According to the Energy Institute report,[4] in 2023, the combustion of fossil fuels by these sectors contributed to 87% of total CO_2 emissions, with the transportation sector having the largest increase in 2023 compared to 2022, achieving a total of 18% of global CO_2 emissions.[5,6] Thus, owing to its significant reliance on fossil fuels, the transport sector stands out as a critical area for sustainable

development. In this sense, the search for renewable energy has become more pressing than ever, with an emphasis on biofuels, which include bioethanol, biogas, and biodiesel.[7–9]

Among biofuels, biodiesel has shown promise as an alternative to fossil fuel-derived diesel owing to its similar physicochemical properties. Moreover, it presents several benefits, such as lower toxicity, biodegradability, lower emissions of greenhouse gases, higher combustion efficiency, flash point, and improved lubricity.[10,11] Biodiesel, defined as a long-chain fatty acid mono-alkyl ester, can be produced mainly through blending, pyrolysis, microemulsion, and transesterification. The latter is the preferred method used in the industrial process due to its economic feasibility, mild reaction conditions, and high yield.[12,13] This process involves the reaction of an alcohol, such as methanol or ethanol, with triglycerides in the presence of a catalyst. Vegetable oils, animal fats, and microalgae are commonly reported as feedstock for biodiesel production, with vegetable oils, specifically edible oils, being the main source used industrially, accounting for 95% of worldwide production.[14]

Nonetheless, the use of edible oils as feedstock has raised many concerns related to deforestation, competition for arable land, and the price of the final product.[10,13] Indeed,

[a] Department of Chemistry and Biochemistry, Concordia University and the Centre for NanoScience Research, Montreal, QC H4B 1R6, Canada.
E-mail: rafik.naccache@concordia.ca
[b] Quebec Centre for Advanced Materials, Concordia University, Montreal, QC H4B 1R6, Canada

This journal is © The Royal Society of Chemistry 2025

Catal. Sci. Technol., 2025, **15**, 6499–6512 | **6499**

the feedstock accounts for about 60–80% of the total production cost, and the use of edible oils has led to an increase in the final product price, which has hindered its global adoption, as it is still more expensive than traditional diesel.[15,16] As such, the search for alternative feedstocks has become critical due to the urgency of transitioning from non-renewable to renewable and sustainable energy sources, with non-edible and waste oils touted as promising alternatives.[17,18] However, these oils present a main disadvantage owing to the presence of high free fatty acid (FFA) content, which impedes the use of homogeneous basic catalysts, such as sodium hydroxide or potassium hydroxide, commonly used in biodiesel production. These conventional basic catalysts are sensitive to moisture and can typically tolerate up to 2% of FFA. Thus, in order to increase the use of non-edible oils in the process, there is a need to shift to acidic catalysts. Homogeneous acid catalysts, such as sulfuric acid, indeed show a higher tolerance to moisture and FFA content; however, these catalysts also present some drawbacks, which include a lower reaction rate, a higher amount of methanol during the reaction, and corrosiveness.[19–21] Heterogeneous acid catalysts have come to light as a promising alternative as they are less corrosive and easier to separate and reuse, resulting in a less intensive purification process, which leads to the generation of less wastewater.[19,22] Transition metal oxides, heteropoly acids, zeolites, metal-doped silica, and sulfonated materials, such as carbon-based materials, are some of the heterogeneous acid catalysts reported in the literature.[20,22]

Sulfonated carbon-based materials have recently garnered attention owing to their sustainability and low-cost synthesis processes. These materials are mainly prepared through pyrolysis, or hydrothermal treatment of widely available biomass waste, or renewable carbon sources, followed by sulfonation treatments using H_2SO_4, chlorosulfonic acid, and p-toluenesulfonic acid (p-TsOH). Moreover, these materials offer several advantages, including high thermal stability, porosity, tunable surface, and strong acidity, comparable to their homogeneous counterpart, sulfuric acid.[13,23–26] In this regard, these materials have emerged as a promising and suitable catalyst for the production of biodiesel, as they can lead to a more economical and greener process owing to the low cost of the raw materials used in their synthesis and the possibility of using low-grade oils. Numerous studies have demonstrated the potential of sulfonated carbon-based material derived from biomass for biodiesel production. Zhang et al.[27] reported an ordered mesoporous carbon catalyst derived from glucose and glycerol for the esterification of an acidic oil, obtaining a conversion of 95%. Karmakar et al.[28] reported a conversion of 92% of castor oil using a sulfonated carbon-based catalyst obtained from Mesua ferrea Linn seed shell. A sulfonated lemon peel-based catalyst was used by Yadav and Ahmaruzzaram[29] for the esterification of oleic acid, achieving a conversion of 96%. Recently, Ruatpuia et al.[30] reported the conversion of Jatropha oil into biodiesel using a glucose-derived sulfonated catalyst. Hamilton et al.[31] also demonstrated the potential of sulfonated lignin as a catalyst for the esterification of oleic acid, showing a conversion of 97%. The first sulfonated carbon-based materials were synthesized from carbohydrates, such as glucose, and have since been widely investigated.[30,32–40] Given their renewable nature, wide availability, low cost, and biodegradability, carbohydrates have attracted significant attention as promising sources for synthesizing carbon sphere-based materials.[41–50] Nonetheless, these materials are synthesized mainly through conventional hydrothermal carbonization, which demands longer reaction times and is highly energy-consuming. In this sense, microwave-assisted hydrothermal carbonization has attracted attention lately owing to its faster and more uniform heating. This reduces reaction time, leading to an improvement in the energy efficiency of the process. In addition, the reaction parameters can be better controlled, rendering improved reproducibility, higher yields, and fewer by-products.[51,52]

In this study, we report a one-pot synthesis of sulfonated carbon-based materials derived from sucrose and their application as a solid acid catalyst for the esterification of oleic acid. The sulfonated carbon-based catalysts were comprehensively characterized, focusing on their acidity to better understand their catalytic activity. Furthermore, we aimed to tailor the surface chemistry of the sulfonated carbon-based materials to enhance their catalytic activity and improve the efficiency of the biodiesel synthesis. Finally, the most effective material was tested as a catalyst to evaluate the influence of oil-to-methanol ratio, catalyst loading, temperature, and reaction time on the esterification of oleic acid.

Methods

Materials

Sucrose (≥99.5%), p-toluenesulfonic acid (≥98.5%), oleic acid (technical grade, 90%), and methanol (≥99.8%) were purchased from Sigma-Aldrich.

Synthesis and optimization of the sulfonated carbon-based catalysts

Sulfonated carbon-based catalysts were synthesized using a one-step microwave-assisted hydrothermal carbonization method. Briefly, sucrose (0.25 M), p-TsOH, and 50 mL of water were mixed in a Teflon vessel, adjusting the mass ratio of sucrose and p-TsOH (1:0.5, 1:1, 1:1.5, and 1:2). The vessel was sealed and heated to the desired temperature (140–220 °C) in a MARS 6 CEM Microwave Digestion System. The reaction time was varied from 10 to 30 minutes. The resulting solids were filtered and washed with distilled water to a neutral pH, followed by organic washes with ethanol in order to eliminate any unreacted precursors. The solids were then dried overnight at 80 °C. The samples were named SSO$_3$H_X:Y_Z_W, where X:Y represents the mass ratio of sucrose and p-TsOH, while Z represents the temperature, and

6500 | Catal. Sci. Technol., 2025, 15, 6499–6512

This journal is © The Royal Society of Chemistry 2025

W represents the time required for the synthesis of the catalyst.

Catalyst characterization

Scanning electron microscopy (SEM) images were obtained on a Phenom ProX desktop SEM. Fourier-transformed infrared (FT-IR) spectra were obtained using a Thermo Scientific Nicolet iS5 equipped with an iD5 ATR accessory between 400 and 4000 cm^{-1}. Thermogravimetric analyses (TGA) were carried out using a TGA Q500 analyser. Samples were heated from 25 to 900 °C at a heating rate of 5 °C min^{-1} under argon atmosphere with a flow rate of 50 mL min^{-1}. Powder X-ray diffraction (PXRD) patterns of the catalysts were obtained on a Rigaku MiniFlex 6G equipped with Cu Kα radiation at 40 kV and 15 mA. The samples were scanned over a range of $10° < 2\theta < 60°$ at a scan rate of 10° min^{-1}. The surface area of the materials was obtained by adsorption/desorption isotherms of N$_2$ at 77 K using a Micrometrics Tristar II Plus. The samples were activated prior to analysis at 100 °C for 24 h, under vacuum. The surface area was calculated using the Brunauer–Emmett–Teller (BET) method. X-ray photoelectron microscopy (XPS) analysis was performed using a Thermo Scientific K-Alpha X-ray photoelectron spectrometer, where each analysis was carried out in triplicate on three different points, with three scans for each sample. The averages were plotted for both the survey and high-resolution scans. ^{13}C cross-polarization (CP)/magic angle spinning (MAS) Nuclear Magnetic Resonance (NMR) spectrum was measured on a Bruker Avance III-HD operating at a frequency of 150.87 MHz for ^{13}C and 599.95 MHz for proton (^{1}H) using a Varian 3.2 mm magic-angle spinning (MAS) triple resonance probe. The spinning frequency was set to 10 kHz, and the probe was kept at room temperature. 1D (single-pulse (SP) and cross polarization (CP)) experiments were recorded with nutation frequencies of 75 kHz and 85 kHz for carbon and proton channels, respectively. Sulfonic acid group content was quantified *via* titration, where 40 mg of catalyst was mixed with 20 mL of 1 M sodium chloride (NaCl) solution for 24 h. The supernatant was then filtered and titrated with 0.001 M sodium hydroxide (NaOH), using phenolphthalein as an indicator. The sulfonic group density is expressed in terms of mmol g^{-1} of catalyst. Similarly, total acid sites were calculated from back titration, where 40 mg of catalyst was mixed with 20 mL of 0.005 M NaOH for 4 hours. The resultant solution was back-titrated against 0.005 M HCl in order to determine the excess of NaOH using phenolphthalein as an indicator.[34,53,54] The acidity of the materials was then determined by the difference between the initial amount and the excess of NaOH and is expressed in terms of mmol g^{-1} of catalyst.

Catalytic activity

The catalyst activity was evaluated towards the esterification of oleic acid (OA) with methanol. The reactions were carried out under conventional heating in an oil bath using crimped vials, with continuous stirring at 600 rpm. A specific amount of the sulfonated carbon-based material (1–7 wt% of OA) was added to methanol and 0.67 mL of OA. Upon reaction completion, the mixture was centrifuged at 10 000 × *g* for 5 min. The top phase, comprising methanol, was evaporated, and the final product obtained was analysed. To ensure the reproducibility of the results, all reactions were carried out in triplicate. Conversion was determined by Proton Nuclear Magnetic Resonance (^{1}H NMR) spectroscopy using a Bruker Fourier Ultrashield™ operating at 300 MHz. All samples were prepared in CDCl$_3$ for analysis. The quantification was calculated using eqn (1),[55]

$$C(\%) = 100 \times (2 \times A_{CH3})/(3 \times A_{CH3}) \tag{1}$$

where $C(\%)$ is the percentage of conversion of oil to biodiesel, A_{CH3} is the integration value of the methoxy protons of the methyl esters at a chemical shift of 3.6 ppm, and A_{CH2} is the integration value of the proton of the α-methylene groups present in both the triglyceride and methyl ester at a chemical shift of 2.3 ppm (Fig. S1).

Results and discussion

Optimization of catalyst synthesis parameters

The synthesis of sulfonated carbon-based materials typically involves the incomplete carbonization or post-sulfonation of the carbon matter with strong sulfonating agents, such as H$_2$SO$_4$ and ClSO$_3$H. Although effective, these methods often require harsh conditions and generate large amounts of acidic waste.[56,57] In this study, *p*-TsOH, a milder and more sustainable alternative, was used as an *in situ* sulfonating agent. This allows simultaneous carbonization and sulfonation of the carbon matter in a single-step synthesis. This approach renders the process more sustainable and greener by reducing the use of corrosive and hazardous agents such as concentrated H$_2$SO$_4$ and avoiding multistep processes.[57–59]

In order to optimize the synthesis of the sulfonated materials, the influence of parameters, such as sucrose : *p*-TsOH mass ratio, reaction temperature, and time on the catalytic activity was investigated (Fig. 1a). For initial studies, a 1 : 9 OA-to-methanol ratio was used. The reaction temperature was maintained at 90 °C for 3 h, and a catalyst loading of 5 wt% (of the mass of OA) was used. All the reactions were performed in triplicate to ensure the reproducibility of the results. The first parameter studied was the effect of the mass ratio (Fig. 1b and S2). The materials were synthesized at 180 °C for 20 minutes while the mass ratio varied from 1 : 0.5 to 1 : 2. Conversion increased from 64.7% to 90.3% as the sucrose : *p*-TsOH mass ratio increased from 1 : 0.5 to 1 : 2. The increase in conversion is likely associated with the increase of –SO$_3$H sites being incorporated onto the carbonaceous structure with the increase of sulfonating agent. However, no significant improvement in catalytic activity was observed when the ratio increased from 1 : 1.5 (90.2%) to 1 : 2 (90.3%), which may be
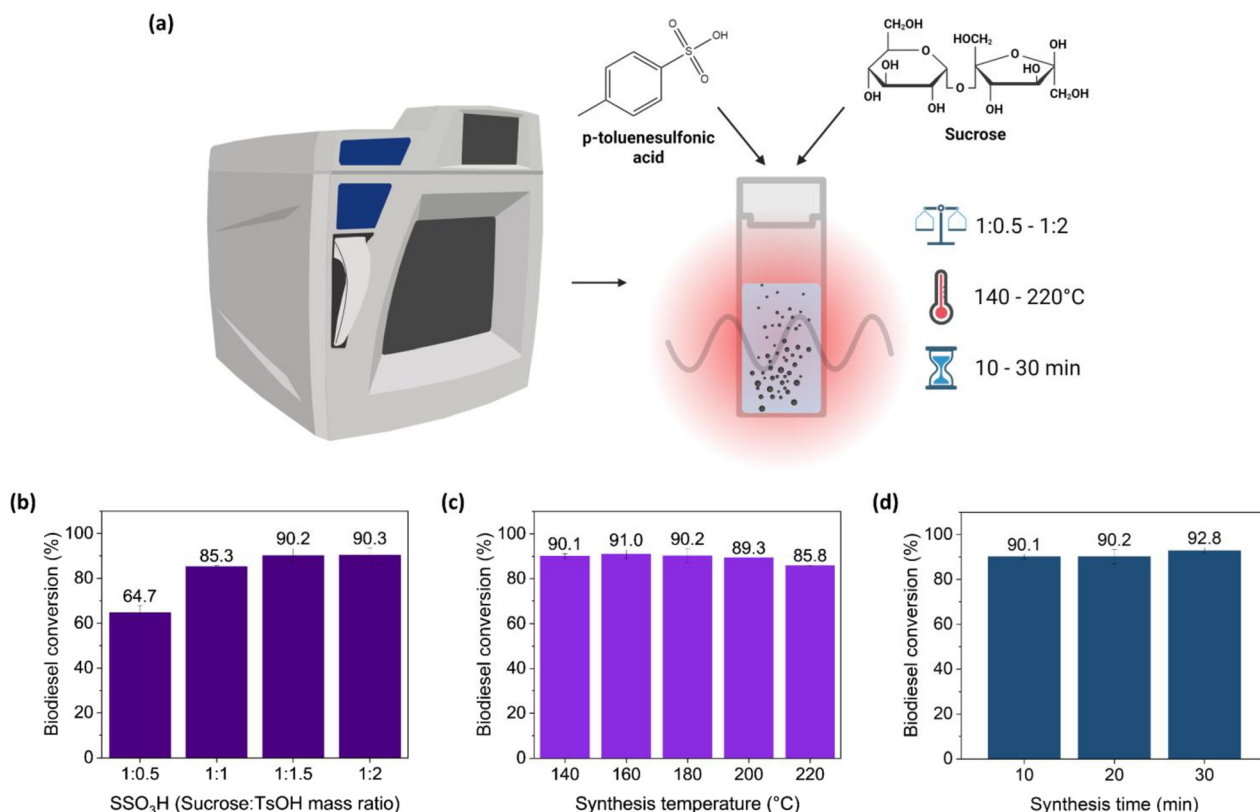
Fig. 1 (a) Scheme depicting the optimization of the microwave-assisted synthesis of sulfonated carbon-based materials. (b) Sucrose : p-TsOH mass ratio (1 : 0.5 to 1 : 2), (c) temperature of synthesis (140 °C to 220 °C), and (d) time of synthesis (10–30 minutes). Biodiesel reaction conditions: molar ratio of OA : methanol of 1 : 9, catalyst loading of 5 wt%, reaction temperature of 90 °C and reaction time of 3 h.

associated with the saturation of the material's surface.[60,61] Niu et al.[60] and Tang et al.[61] reported similar results, where a decrease in conversion was observed after a certain amount of sulfonating agent was added, related to the mass of carbonaceous material. As a result, a mass ratio of 1 : 1.5 (sucrose to p-TsOH) was determined as optimal for further investigations. The effect of the temperature was then evaluated, varying from 140 °C to 220 °C while keeping the reaction time at 20 minutes and the mass ratio at 1 : 1.5 (Fig. 1c and S3). No significant differences in conversion were observed when the temperature increased from 140 °C to 180 °C. However, a slight decrease was observed when the reaction temperature was increased to 200 °C and 220 °C. The decrease in catalytic activity may be associated with the degradation of –SO$_3$H sites and the agglomeration of the carbon sphere structure.[43,56] Thus, in order to determine the optimal synthesis temperature, an additional analysis considering the material yield and energy efficiency was performed (Fig. S4 and Table S1). As can be seen, the yield almost doubled when the temperature was increased from 140 °C to 160 °C. However, between 160 °C and 180 °C, the yield increased by about 33%, while a slight increase (8%) was observed from 180 °C to 200 °C. A similar trend was observed for the energy consumed per gram of material produced. The energy consumed at 140 °C was approximately double that at 160 °C. Nonetheless, between 160 °C and 180 °C, a drop of about 25% in energy

consumption is observed, while the energy consumed per gram of material seems to reach a plateau after 180 °C. Thus, 180 °C was selected as the optimum temperature, as it showed a good balance between catalyst yield and energy efficiency. The last parameter evaluated was the effect of the synthesis time, ranging from 10 to 30 minutes, maintaining the mass ratio at 1 : 1.5 and the temperature at 180 °C (Fig. 1d and S5). No significant increase in conversion was observed when the time was extended from 10 to 30 minutes. Thus, an additional analysis considering the material yield and energy efficiency was performed to determine the optimal synthesis time (Fig. S6 and Table S2). An increase in yield of about 11% was observed when the reaction time was extended from 10 to 20 minutes, while the gain in yield between 20 and 30 minutes was only about 4%. This trend was also observed in the energy consumption per gram of catalyst. The increase in the energy consumed per gram of material was about 81% when the reaction time was increased from 10 to 20 minutes, resulting in an additional energy cost of 4.81×10^3 kJ g^{-1}. Increasing the reaction time to 30 minutes led to a higher additional energy cost of about 1.05×10^4 kJ g^{-1} and an increase in energy per gram of approximately 44%. Although the total energy input doubled from 10 to 20 min, the increase in yield justifies the trade-off between energy input and yield. Furthermore, the slightly higher yield at 20 min provides more material per batch, reducing the need for multiple syntheses to obtain

6502 | Catal. Sci. Technol., 2025, **15**, 6499–6512

This journal is © The Royal Society of Chemistry 2025

sufficient material for subsequent reactions, which would have increased the total energy consumption of the process. Therefore, 20 min was chosen as the optimal synthesis time, and the corresponding material SSO$_3$H_1:1.5_180_20 was used for further optimization of the OA esterification. Control syntheses of the materials using either only sucrose or p-TsOH were also performed under the same conditions defined previously (180 °C, 20 min), but no solid was obtained.

Moreover, to compare the energy efficiency between microwave-assisted synthesis and conventional hydrothermal synthesis, reactions were carried out under the same conditions of sucrose : p-TsOH mass ratio, temperature, and time in a hydrothermal reactor. No solids were obtained, confirming the advantage of microwave heating in accelerating carbonization and sulfonation processes. Therefore, syntheses were carried out with longer reaction times, such as 12 h and 24 h, under the same mass ratio and temperature conditions. Based on the operational data of the muffle furnace used, the energy consumption was estimated as 129 600 kJ for the 12 h reaction and 259 200 kJ for the 24 h counterpart. Considering the yield of the reaction, the 24 h synthesis achieved 5.24%, corresponding to an energy consumption of 5.78×10^5 kJ g^{-1} of material, while the 12 h synthesis presented a yield of 5.50%, and an energy consumption of 2.76×10^5 kJ g^{-1} (Table S3). The hydrothermally synthesized materials were also tested as catalysts for the esterification of OA. Comparable conversions of 92.7% and 93.4% for the 12 h and 24 h materials, respectively, were achieved, indicating that the synthesis route did not significantly affect the catalytic activity. However, these findings emphasize the considerable advantages of using the microwave-assisted approach compared to conventional methods of synthesis, owing to its energy efficiency, sustainability, and greener aspect.

Structural analyses and properties

The morphology of the sulfonated carbons was investigated by scanning electron microscopy (SEM) (Fig. 2a and S7). All materials consisted of interconnected microspheres. SSO$_3$H_1:0.5_180_20 presented larger particles, with a *peanut-like* shape, and diameters ranging from 2–17 μm. The increase in mass ratio, temperature, and reaction time led to the formation of smaller spheres, with sizes varying from 1–7 μm. This morphology has been reported for hydrothermal-derived materials synthesized from
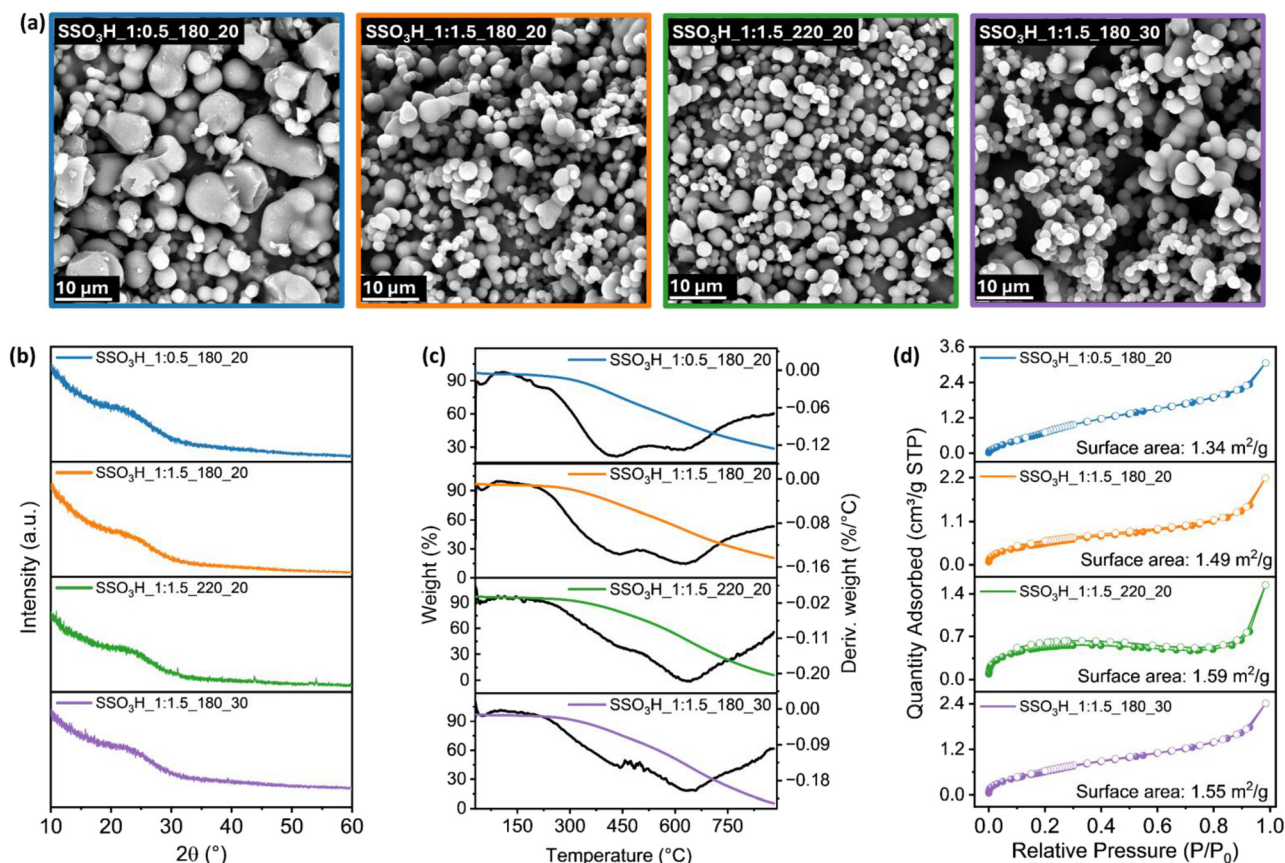

Fig. 2 (a) Scanning electron micrographs of the sulfonated carbon-based materials showed that all materials are composed of interconnected spheres with sizes ranging from 1–17 μm; (b) PXRD pattern of the sulfonated carbon materials, confirming their amorphous nature; (c) TGA curves of the sulfonated carbon based materials showing three mass events associated with the loss of moisture, degradation of sulfonic acid groups and the oxygenated groups, respectively; (d) N$_2$ adsorption/desorption isotherms of the sulfonated materials evidence a type II isotherm and a low BET surface area.

This journal is © The Royal Society of Chemistry 2025

Catal. Sci. Technol., 2025, 15, 6499–6512 | 6503

carbohydrates, such as glucose and sucrose.[42,43,47,62,63] The formation of the spheres typically involves the hydrolysis of the saccharides into monosaccharides, such as glucose and fructose, followed by dehydration and isomerization reactions, which produce intermediates like HMF (5-hydroxymethylfurfural). These intermediates undergo condensation and polymerization reactions, forming aromatic-rich structures that nucleate and grow into spheres.[43,64] Moreover, *p*-TsOH can act not only as a sulfonating agent, but also as a catalyst, increasing the rate of the hydrolysis and dehydration steps.[65,66]

All the PXRD patterns (Fig. 2b and S8a) showed a broad and weak diffraction peak centred at $2\theta \approx 22°$

attributed to the (002) plane of graphite, indicating the amorphous nature of the material.[67,68] The thermal stability of the catalysts was investigated using TGA (Fig. 2c and S8b). All materials presented two main decomposition stages. The first mass loss event of ~4% at 49 °C is attributed to moisture adsorbed on the surface of the materials. Subsequently, a gradual mass loss is observed with the increase in temperature, with two main mass loss events. The first event occurring from 150 °C to 500 °C is attributed to the decomposition of sulfonic acid, while the second event from 500 °C to 750 °C is associated with the decomposition of oxygenated moieties and the carbonaceous structure. Similar results were
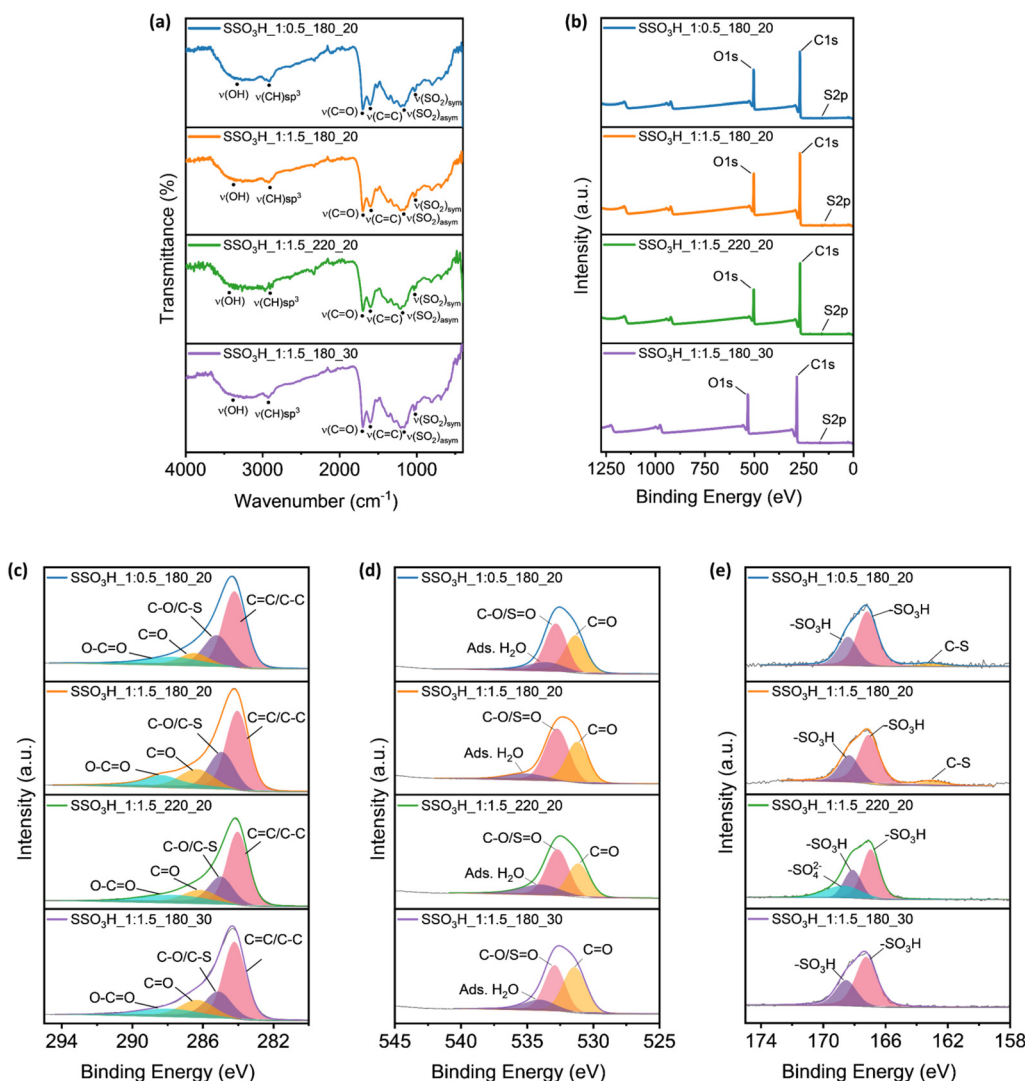

Fig. 3 (a) FTIR spectra of sulfonated carbon materials showing the vibration modes of O–H (3293 cm^{-1}), C–H sp^3 (2915 cm^{-1}), C=O (1702 cm^{-1}), C=C aromatics (1608 cm^{-1}), SO$_2$ asymmetric (1155 and 1286 cm^{-1}) and, SO$_2$ symmetric (1028, 1011 cm^{-1}) bands; (b) XPS survey scan revealing 285 eV, 533 eV and 169 eV binding energies corresponding to carbon (C 1s), oxygen (O 1s), and sulfur (S 2p), respectively. (c) Deconvoluted high-resolution spectra of C 1s showed binding energies at ~284.2 eV, ~285.2 eV, ~286.3 eV, and ~288.3 eV attributed to the C=C, C–O/C–S, C=O, and O–C=O, respectively; (d) deconvoluted high-resolution spectra of O 1s revealed binding energies at 531.3 eV and 532.8 eV representative of C–O/S=O and C=O bonds, respectively; (e) deconvoluted high-resolution spectra of S 2p confirmed the presence of binding energies at 167.2 eV, 168.3 eV, 163.1 eV for some samples and 168.8 eV for SSO$_3$H_1:1.5_220_20, ascribed to S 2p$_{3/2}$ and S 2p$_{1/2}$ of –SO$_3$H, C–S bond and SO$_4^{2-}$ species, respectively.

6504 | *Catal. Sci. Technol.*, 2025, **15**, 6499–6512

This journal is © The Royal Society of Chemistry 2025

reported in studies that investigated the thermal decomposition of sulfonated-carbon materials.[67,69,70]

The BET surface area of the materials was determined by N_2 sorption isotherms (Fig. 2d). All materials showed low surface areas, <2 m^2 g^{-1}, indicating a non-porous structure and corroborating the observed type II isotherm. As reported in previous studies, hydrothermal carbons typically present low surface areas, which agrees with our findings.[43,48,63,71] No significant changes in surface area were observed with the increase in mass ratio, temperature, and reaction time. The presence of the functional groups in the materials was investigated by FTIR (Fig. 3a and S8c). All materials displayed characteristics bands attributed to the stretching mode of O–H (3293 cm^{-1}), C–H sp^3 (2915 cm^{-1}), C=O (1702 cm^{-1}), C=C aromatics (1608 cm^{-1}), SO_2 asymmetric (1155 and 1286 cm^{-1}) and, SO_2 symmetric (1028, 1011 cm^{-1}).[56,71] These results confirm that the sulfonic acid groups were successfully inserted into the structure of the materials. Furthermore, the presence of oxygenated functional groups was also observed. This is consistent with the sulfonation process since it not only introduces sulfonic groups but also functional groups such as –COOH and –OH.[56,67]

To further confirm the functional groups present on the surface of the material, XPS analysis was performed. The survey spectrum revealed peaks corresponding to binding energy associated with C 1s (285 eV), O 1s (533 eV), and S 2p (169 eV) as shown in Fig. 3b and S9a The deconvoluted high-resolution spectrum of C 1s (Fig. 3c and S9b) displayed characteristic peaks at ~284.2 eV, ~285.2 eV, ~286.3 eV and ~288.3 eV ascribed to C=C, C–O/C–S, C=O bonds and O–C=O, respectively. Furthermore, the presence of bonds attributed to C–O (~531.3 eV) and C=O/S=O (~532.8 eV) was further confirmed in the deconvoluted high-resolution spectrum of O 1s (Fig. 3d and S10a). Finally, the deconvoluted high-resolution spectrum of S 2p (Fig. 3e and S10b) confirmed the incorporation of sulfonic acid groups by the presence of peaks centred at 167.2 and 168.3 eV, which are characteristic of –SO$_3$H bonds. A peak at ~163.1 eV, corresponding to C–S bonds, was also observed in some samples, suggesting partial incorporation of sulfur into the material structure. Moreover, materials synthesized at higher temperatures, 200 and 220 °C, presented a peak centred at ~168.8 eV assigned to SO_4^{2-}. This may be associated with the thermal degradation of –SO$_3$H groups into sulfate form, which can contribute to the decrease in catalytic activity observed for these materials.[62,72,73] XPS analysis also revealed an increase in sulfur content with the increase in the molar ratio of sucrose : p-TsOH, as well as with the increase in temperature and time of synthesis (Table S4). These results indicate that the synthesis conditions influence the incorporation of sulfur species into the surface of the carbon matrix. However, the deconvoluted high-resolution spectra of S 2p showed that the sulfur content is not only related to the sulfonic groups but also to other sulfur moieties that do not contribute to the esterification reaction. Thus, in order to quantify accessible and catalytically active sites, acid–

base back titrations were employed. In contrast to the trend observed by XPS, titration did not show a proportional relationship between the increase in the molar ratio of sucrose : p-TsOH, temperature, and reaction time, with the increase in sulfonic groups. This difference is expected, as titration quantifies only the acidic groups that are available for the reaction, whereas XPS is an intrinsic surface technique, measuring all sulfur species, as previously discussed.[56] ^{13}C CP/MAS NMR was performed to further investigate the structure of SSO$_3$H_1 : 1.5_180_20 (Fig. S11). The spectrum showed signals between 10–40 ppm, associated with sp^3 carbons, as well as signals between 114–120 ppm, which are ascribed to polycyclic aromatic carbons. The presence of C–SO$_3$H was also confirmed by the signal at 141 ppm, in addition to –OH, –COOH, and C=O moieties corresponding to the signals at 150, 175, and 206 ppm, respectively. These findings corroborate the FTIR and XPS analyses, further confirming the incorporation of sulfonic and oxygenated groups onto the carbon material.[54,56,74]

The acid–base back titration showed that the number of –SO$_3$H did not change significantly among most samples, varying from 0.18 to 0.22 mmol g^{-1}, except for the material SSO$_3$H_1 : 0.5_180_20 which presented the highest amount of 0.26 mmol g^{-1} as shown in Table 1. However, this material also presented the lowest biodiesel conversion as mentioned previously. This result may be associated with the lower total acidity of this material (1.98 mmol g^{-1}) compared to the other samples. Although –SO$_3$H groups are known to be the main catalytic site for esterification reactions, oxygenated groups, such as COOH and OH, are known to promote a synergetic effect and enhance the material's catalytic activity.[67,75] Moreover, the low conversion can be related to the reduced accessibility of the acid sites owing to the larger particle size observed for this material.[59] It is also possible to observe that an increase in temperature above 180 °C led to a decrease in the number of –SO$_3$H and total acid sites, which is consistent with the biodiesel conversion results shown previously for the materials SSO$_3$H_1 : 1.5_200_20 and SSO$_3$H_1 : 1.5_220_20. This finding is likely attributed to the decomposition of the sulfonic groups and partial degradation of the carbon structure, as confirmed by XPS through the appearance of SO_4^{2-} moieties.

Thus, based on the material optimization studies and the structural and physicochemical properties, the material SSO$_3$H_1 : 1.5_180_20 was selected as the optimal catalyst for optimizing the esterification of oleic acid. This material showed a favourable ratio between the number of –SO$_3$H sites and total acid sites, which contributed to its catalytic activity. In addition, its synthesis conditions provided a balance between yield and energy efficacy.

Catalytic performance towards esterification

The main parameters that affect biodiesel reaction and its yield are oil-to-methanol molar ratio, catalyst loading, temperature, and time, as they directly affect the reaction

This journal is © The Royal Society of Chemistry 2025

Catal. Sci. Technol., 2025, **15**, 6499–6512 | **6505**

Table 1 Density of sulfonic acid and other acid sites on the surface of the sulfonated carbon-based materials

Material	–SO$_3$H (mmol g^{-1})	COOH/OH (mmol g^{-1})	Total acid site (mmol g^{-1})	Biodiesel conversion (%)
SSO$_3$H_1:0.5_180_20	0.26 ± 0.01	1.73 ± 0.02	1.98 ± 0.02	64.7
SSO$_3$H_1:1_180_20	0.22 ± 0.01	1.87 ± 0.03	2.09 ± 0.03	85.3
SSO$_3$H_1:1.5_180_20	0.20 ± 0.01	1.85 ± 0.02	2.05 ± 0.02	90.2
SSO$_3$H_1:2_180_20	0.20 ± 0.00	1.89 ± 0.03	2.09 ± 0.03	90.3
SSO$_3$H_1:1.5_140_20	0.19 ± 0.00	1.93 ± 0.04	2.11 ± 0.04	90.1
SSO$_3$H_1:1.5_160_20	0.21 ± 0.00	1.85 ± 0.02	2.06 ± 0.02	91.0
SSO$_3$H_1:1.5_200 _20	0.18 ± 0.00	1.70 ± 0.03	1.88 ± 0.03	89.3
SSO$_3$H_1:1.5_220_20	0.14 ± 0.01	1.66 ± 0.02	1.81 ±0.02	85.8
SSO$_3$H_1:1.5_180_10	0.20 ± 0.00	1.88 ± 0.01	2.07 ± 0.00	90.1
SSO$_3$H_1:1.5_180_30	0.18 ± 0.02	1.73 ± 0.03	1.92 ± 0.02	92.8

kinetics and the efficiency of the conversion of the oil or fatty acid into biodiesel.[76–79] Thus, the One Variable at a Time (OVAT) method was applied to investigate the effect of each parameter and to optimize the reaction conditions using the selected material, SSO$_3$H_1:1.5_180_20. The first parameter investigated was the molar ratio of oleic acid to methanol (Fig. 4a and S12). Although the reaction of oleic acid with methanol requires a molar ratio of 1:1, esterification is a reversible reaction, making the use of an excess of methanol necessary to shift the equilibrium toward the product side and consequently improve the reaction yield.[76] Therefore, identifying an optimal ratio is essential to achieve high conversions while minimizing solvent waste. To evaluate this parameter, the reactions were carried out by varying the ratios from 1:6 to 1:30, while the catalyst loading, temperature, and reaction time were maintained constant (5 wt%, 90 °C, and 3 h). When the OA to oil molar ratio was 1:6, a conversion of 82.5% was achieved, while increasing to 1:9 and 1:12 led to a slight increase to ~90%. However, upon increasing the ratio to 1:18, the conversion increased to 95.4%, with no significant improvement observed at higher molar ratios. Therefore, the optimal oleic acid to methanol ratio was determined to be 1:18. After the molar ratio optimization, the effect of catalyst loading was investigated. Although esterification reactions can occur without a catalyst, the reaction rate is significantly slower. For this reason, the use of catalysts is essential to enhance the reaction rate.[88] Heterogeneous acid catalysts offer significant advantages over their homogeneous counterparts but often require higher catalyst loading, typically up to 15 wt%, whereas the homogeneous counterparts can achieve high conversion with just 1 wt% or less.[20,89] In order to assess the effect of this parameter, the reactions were performed with catalyst loadings ranging from 1 to 7 wt%, while maintaining the other parameters constant (1:18 molar ratio, 90 °C, and 3 h) (Fig. 4b and S13). A conversion of about 55% was obtained with 1 wt% of catalyst, while increasing the catalyst loading to 3 wt% led to an improvement in the conversion, achieving a biodiesel conversion of 84.5%. The highest conversion (95.4%) was achieved upon increasing the catalyst loading to 5 wt%. However, a further increase to 7 wt% showed no enhancement in conversion but rather a slight decrease. This finding may be associated with an excess of catalyst, which, being in a different phase from the reaction medium, can cause particle agglomeration and increase mass transfer resistance, a common limitation faced with the use of heterogeneous catalysts. Thus, 5 wt% of catalyst loading was selected for further optimizations.

Esterification reactions are endothermic, and an increase in temperature normally increases conversion. The rise in reaction temperature not only favours the collision between the molecules but also reduces the viscosity of the reaction medium, lowering the mass transfer resistance.[90,91] Therefore, the temperature effect on the catalytic activity of SSO$_3$H_1:1.5_180_20 was evaluated. The reactions were performed at 70, 80, and 90 °C, under the conditions of 1:18 molar ratio, 5 wt% catalyst loading, and reaction time of 3 h (Fig. 4c and S14). As expected, the increase in temperature results in an enhancement in conversion, rising from 75.1% at 70 °C to 95.4% at 90 °C. Hence, 90 °C was chosen as the optimal temperature. The last parameter investigated was the reaction time. This variable plays a significant role in the conversion, as short reaction times may not allow complete miscibility and sufficient collisions between the oil and methanol molecules, resulting in lower yields. However, as previously mentioned, esterification is a reversible reaction; thus, long reaction times may also result in low yields as they may promote the reverse reaction. Therefore, it is crucial to determine the optimal time to ensure high conversion rates.[90] The effect of the time on the catalytic activity was studied, varying it from 30 minutes to 5 h (Fig. 4d and S15) while keeping the previously optimized parameters constant (1:18 molar ratio, 5 wt% catalyst loading, and 90 °C). It was observed that the increase in time resulted in a slight increase in conversion, with the highest biodiesel conversion achieved (97.6%) at 5 h. However, it is worth mentioning that approximately 91% of the oleic acid was converted within the first 30 minutes of reaction, demonstrating the remarkable activity of the material. A comparison with previously sulfonated carbon-based materials reported in the literature is presented in Table 2. Although some studies showed higher biodiesel conversion, they required longer reaction times, higher catalyst loadings, and/or higher temperatures, while a 91% conversion was achieved using SSO$_3$H_1:1.5_180_20 under

6506 | Catal. Sci. Technol., 2025, 15, 6499–6512

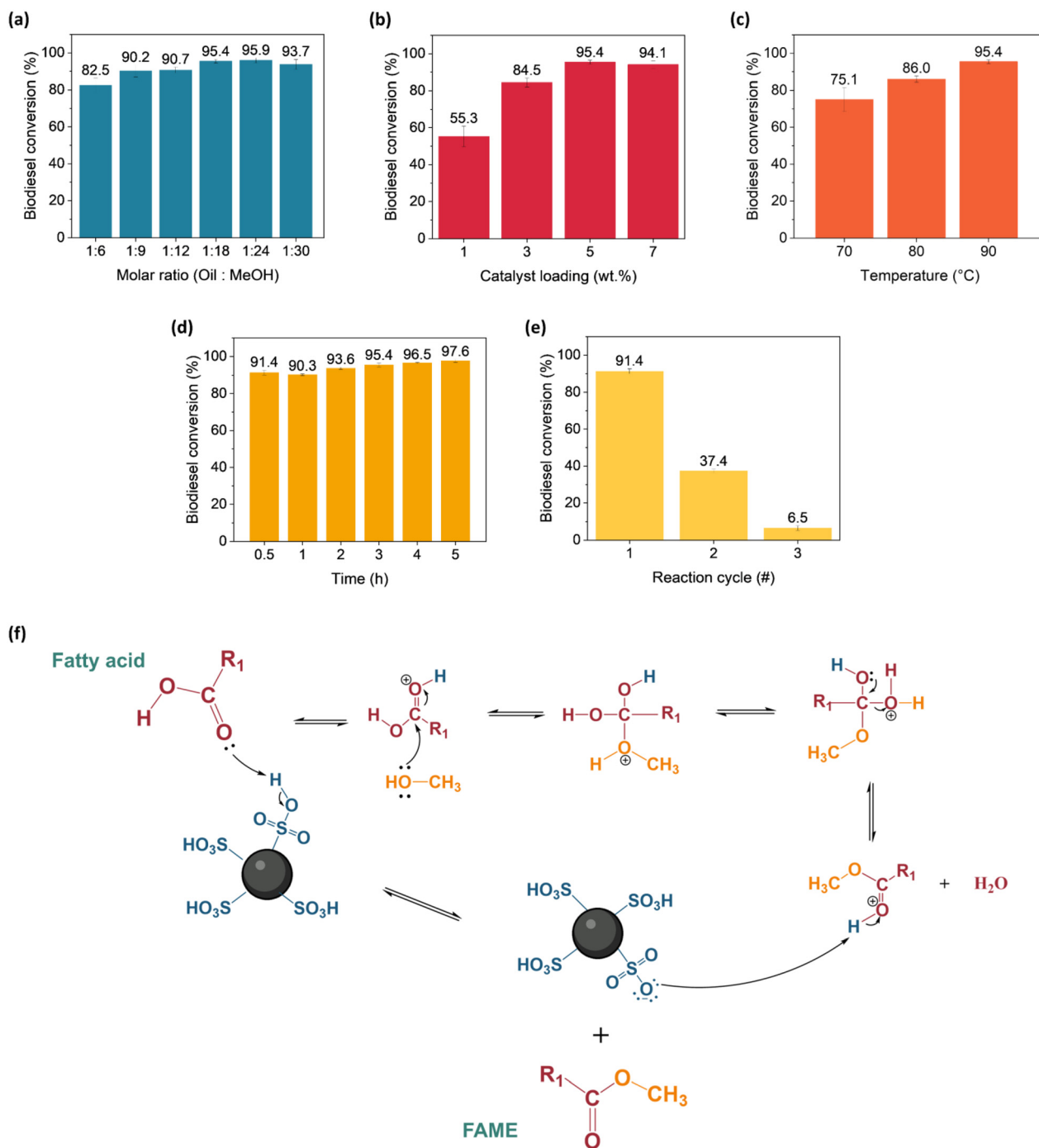This journal is © The Royal Society of Chemistry 2025

Fig. 4 (a) Reaction optimization of oil:methanol molar ratio, (b) catalyst loading (wt%), (c) temperature (°C), and (d) reaction time. (e) Reusability test of SSO$_3$H_1:1.5_180_20 for the esterification reaction. (f) Proposed esterification mechanism using SSO$_3$H_1:1.5_180_20 as a catalyst.

mild conditions (1:18 molar ratio, 5 wt%, 90 °C, and 30 min). Moreover, SSO$_3$H_1:1.5_180_20 was easily obtained using a one-pot, microwave-assisted *in situ* sulfonation. This approach avoided long reaction times commonly employed in conventional hydrothermal and post-sulfonation methods, rendering it a simpler and more energetically viable process.

In order to study the catalyst reusability and the stability of sulfonic acid groups, the solid was recovered after the completion of the reaction after each cycle, washed with

hexane and acetone, and finally dried (Fig. 4e and S16). Reuse tests were performed under the conditions of 1:18 molar ratio, 5 wt% catalyst loading, 90 °C and 30 minutes. Although the highest conversion was achieved at 5 h, 30 min was selected for the reuse tests as it provides satisfactory conversion, but also offers a more energy-efficient process. A significant reduction in conversion is observed after the second cycle, decreasing from 91.4% to 37.4%. A further decrease is observed in the third cycle, where the conversion

This journal is © The Royal Society of Chemistry 2025

Catal. Sci. Technol., 2025, **15**, 6499–6512 | **6507**

Table 2 Comparative study of the reaction conditions and biodiesel conversion obtained in the esterification reaction using sulfonated carbon-based catalyst

Catalyst	Synthesis method	–SO$_3$H acidity (mmol g^{-1})	Esterification conditions (molar ratio, catalyst loading, temperature, time)	Conversion (%)	Reference
Sulfonated açaí seeds	Hydrothermal carbonization (190 °C, 24 h) + sulfonation (100 °C, 1 h)	2.3	1 : 12, 5 wt%, 100 °C, 1 h	91.0	62
Chitosan	In situ hydrothermal carbonization–sulfonation (H$_2$SO$_4$, 180 °C, 5 h)	3.4	1 : 18.7, 4.4 wt%, 82 °C, 4.3 h	98.6	80
Cacao shells	In situ carbonization–sulfonation in digestion system (120 °C, 6 h)	0.85	1 : 7, 7 wt%, 65 °C, 24 h	76.0	81
Palm leaf waste	Hydrothermal carbonization (200 °C, 12 h) + sulfonation (150 °C, 6 h)	7.35[a]	1 : 18, 4 wt%, 80 °C, 4 h	93.56	82
Corncob	Hydrothermal carbonization (190 °C, 24 h) + sulfonation (100 °C, 1 h)	2.63	1 : 15, 3 wt%, 70 °C, 2 h	92.0	83
Murumuru kernel shell	Carbonization (600 °C, 1 h) + sulfonation (200 °C, 4 h)	4.2[a]	1 : 10, 5 wt%, 90 °C, 1.5 h	97.2	67
Glucose	In situ hydrothermal carbonization–sulfonation (p-TsOH, 180 °C, 24 h)	1.99[a]	1 : 80, 0.1 g,[b] 80 °C, 4 h	99.0	84
Magnetic açaí seeds	Carbonization (400 °C, 3 h) + sulfonation (80 °C, 3 h)	0.74	1 : 12, 5 wt%, 100 °C, 1 h	88.0	85
Bamboo powder	In situ carbonization–sulfonation in digestion system (150 °C, 4 h)	1.41	1 : 8, 10 wt%, 65 °C, 5 h	97.98	86
Glucose	In situ hydrothermal carbonization–sulfonation (H$_2$SO$_4$, 80 °C, 18 h)	1.29	1 : 20, 5 wt%, 80 °C, 120 min	97.5	87
Sucrose	Microwave-assisted in situ sulfonation (p-TsOH, 180 °C, 20 min)	0.20	1 : 18, 5 wt%, 90 °C, 30 min	91.4	This study

[a] Total acid density. [b] Catalyst loading not provided as the reaction was performed with succinic acid.

drops to 6.5%. These findings may be attributed to the leaching of sulfonic groups and/or partial dissolution of polyaromatic moieties of the material structure, in addition to the formation of sulfonated esters and ion-exchange of the proton with the reaction media.[23,56,92] Titrations of the material were carried out to determine the density of –SO$_3$H groups after each reaction cycle. As expected, the titrations confirmed the progressive loss of the –SO$_3$H group, lowering from 0.20 mmol g^{-1} in the fresh catalyst to 0.11 mmol g^{-1} after the second reuse (Fig. S17), corroborating the observed decline in catalytic activity. The rapid deactivation observed may be associated with the relatively low density of –SO$_3$H groups (0.20 mmol g^{-1}) in the fresh material when compared to materials reported in the literature, which typically range around 0.6 mmol g^{-1}. Nevertheless, despite having fewer acidic sites, the material still demonstrated remarkable catalytic activity for one reaction cycle.

The deactivation of sulfonated carbon-based materials is commonly reported in the literature and remains one of the main challenges associated with their use and reuse in esterification reactions. According to Konwar et al.,[56] the instability of these groups is strongly influenced by the structural feature of the carbon matrix. Materials with low aromaticity or insufficient polycondensation have weaker C–S bonds, which facilitate the leaching of sulfonic groups under reaction conditions. Thus, efforts to make these materials more stable and to regenerate them have recently intensified. The approaches reported include the increase in the aromatic character of the carbon backbone to enhance the anchoring of sulfonic groups and the introduction of oxygenated

functionalities, such as –OH or –COOH, prior to sulfonation to provide additional binding sites. In addition, resulfonation of the spent material to restore its acidity has been explored.[24,93]

Although SSO$_3$H_1 : 1.5_180_20 did not exhibit good reusability, it is important to emphasize the advantages of the method used to synthesize the material compared to those commonly reported. In contrast with the conventional hydrothermal method, the synthesis in this study was completed in only 20 minutes using a microwave-assisted method and in situ sulfonation. This highlights the potential of this approach for a rapid and more sustainable process.

Thus, the results presented in this work demonstrate the potential of the method used for catalyst synthesis to make the biodiesel process more economically feasible and sustainable. The catalyst was obtained from a renewable and low-cost precursor combined with a less hazardous sulfonating agent. Moreover, the microwave reactor allowed the synthesis time to be reduced from more than twelve hours, required in conventional hydrothermal synthesis, to only twenty minutes, which results in a significant decrease in energy consumption. Consequently, the approach has the potential to reduce the cost of catalyst preparation and contribute to making biodiesel production more competitive.

Furthermore, the simplicity of the method and the short synthesis time required make it attractive for large-scale applications. However, recent studies have reported that microwave scale-up is not a straightforward process. The main limitations are related to the limited penetration depth of microwave radiation in the materials and, consequently,

6508 | Catal. Sci. Technol., 2025, **15**, 6499–6512

This journal is © The Royal Society of Chemistry 2025

the challenge of achieving uniform heating, as well as the need for dedicated reactor designs and equipment configurations to handle larger volumes. Despite these limitations, the scale-up of this technology has gained attention due to its potential to render processes more energy-efficient.[52,94]

Reaction mechanism

As previously discussed, FTIR and XPS analyses confirmed the presence of $-SO_3H$ groups through characteristic SO_2 stretching bands, and S 2p binding energies at 167.2 and 168.3 eV. The $-SO_3H$ group is well known to be a strong Brønsted acid, and, consequently, acts as the main catalytic site for the esterification reaction. Moreover, the presence of oxygenated groups, such as $-COOH$ and $-OH$, was also confirmed *via* these analyses. Those groups are considered weak acids and play a synergetic role with their $-SO_3H$ counterparts during the esterification reaction. Thus, based on these surface properties, a Brønsted acid-catalysed mechanism for the esterification of oleic acid was proposed, as detailed in Fig. 4f. The first step is the protonation of the fatty acid by the $-SO_3H$ groups, followed by the nucleophilic attack of methanol on the carboxyl carbon, forming a tetrahedral intermediate. Subsequently, a proton transfer converts the $-OH$ group into a good leaving group. The double bond of the carboxyl is regenerated, leading to the elimination of water and the formation of the conjugated acid of the ester. Finally, the sulfonate ion attacks the proton in the conjugated acid of the ester, recovering the catalyst structure and forming the fatty acid methyl ester (FAME).

Conclusions

The results obtained in this work demonstrated that a sulfonated carbon-based catalyst derived from sucrose is a promising alternative for the esterification of oleic acid for biodiesel production. The catalyst exhibited high efficiency combined with a simple and low-energy-demand synthesis, especially through the use of a microwave-assisted approach. This method significantly reduced synthesis time compared to conventional hydrothermal treatments, which typically require several hours and consume more energy. A comprehensive study of the synthesis parameters identified the optimal condition as a 1:1.5 sucrose to *p*-toluenesulfonic acid mass ratio, at 180 °C for 20 minutes. SSO₃H_1:1.5_180_20 was also synthesized *via* conventional hydrothermal carbonization under the same optimal conditions of mass ratio, temperature, and time, in order to perform a quantitative comparison of energy efficiency between the two methods. It was observed that, under microwave heating, solids were obtained in 20 minutes with an estimated energy consumption of 960 kJ, while no solids were formed under the same conditions for the hydrothermal approach. Therefore, materials were synthesized using longer reaction times, and the energy consumption was estimated at 129 600 kJ and 259 200 kJ for

12 h and 24 h of hydrothermal syntheses, respectively. These findings confirmed the advantage of using microwave-assisted synthesis over conventional hydrothermal one.

Acid–base titrations confirmed the successful incorporation of sulfonic groups on the material surface, with a $-SO_3H$ density of 0.20 mmol g^{-1} and a total acidity of 2.05 mmol g^{-1}. This material achieved 90.2% conversion in preliminary esterification tests. Subsequently, using a one-variable-at-a-time (OVAT) approach, main reaction parameters such as the molar ratio of oleic acid to methanol, catalyst loading, temperature, and reaction time were optimized. The optimal esterification conditions were determined to be a 1:18 oil-to-methanol ratio, 5 wt% catalyst loading, 90 °C, and 30 minutes, achieving a conversion of 91.4%. Conversions up to 95.4% were reached with longer reaction times. However, the catalyst's strong performance under milder and faster conditions renders it particularly attractive compared to other systems requiring harsher reaction parameters. Reusability tests showed a significant drop in performance after the second cycle, likely due to partial leaching of sulfonic groups. Nevertheless, the catalyst's low cost, rapid and energy-efficient synthesis, and excellent performance under mild conditions highlight its potential for more sustainable and practical biodiesel production.

In this context, considering the potential of the material synthesized in this study and the advantages of the method of synthesis applied, evaluating its performance with low-grade feedstocks and assessing the scalability of the process are promising future directions to be explored. Moreover, strategies to improve the stability of SSO3H_1:1.5_180_20 and increase its acidity, such as the use of polyphenolic compounds as carbon precursors during the synthesis, should be considered, as they can act as cross-linkers and increase not only the number of oxygenated groups but also the aromaticity of the material.

Data availability

Supplementary information: ^{1}H NMR assignments for oleic acid and biodiesel, ^{1}H NMR spectra of the obtained products, yield and energy consumption analyses, additional SEM, PXRD, TGA, FTIR and XPS analyses, ^{13}C CP/MAS NMR spectrum of SSO₃H_1:1.5_180_20, density of sulfonic acid groups after reusability test. See DOI: **https://doi.org/10.1039/D5CY00736D**.

The authors confirm that the data supporting the findings of this manuscript are available within the article and its SI.

Author contributions

M. P. D.: conceptualization, methodology, investigation, formal analysis, writing – original draft, writing – review and editing; L. P.: conceptualization, methodology, investigation,

This journal is © The Royal Society of Chemistry 2025

Catal. Sci. Technol., 2025, **15**, 6499–6512 | **6509**

References

1 S. Jha, S. Nanda, B. Acharya and A. K. Dalai, in *Biomass to Bioenergy: Modern Technological Strategies for Biorefineries*, Woodhead Publishing, 2023, pp. 1–14.

2 P. Rath, M. Jindal and T. Jindal, *Clean. Eng. Technol.*, 2021, **5**, 100318.

3 N. K. Arora and I. Mishra, *Environ. Sustainability*, 2019, **2**, 339–342.

4 EI - Energy Institute, *Statistical Review of World Energy*, 2024.

5 International Energy Agency, *CO2 Emissions in 2023*, Paris, 2023.

6 M. Crippa, D. Guizzardi, F. Pagani, M. Banja, M. Muntean, E. Schaaf, F. Monforti-Ferrario, W. Becker, R. Quadrelli, A. Risquez Martin, P. Taghavi-Moharamli, G. Köykkä, J. Grassi, S. Rossi, J. Melo, D. Oom, A. Branco, J. San-Miguel, G. Manca, E. Pisoni, E. Vignati and F. Pekar, *GHG emissions of all world countries*, Luxembourg, 2024.

7 K. Dhandayuthapani, P. S. Kumar, W. Y. Chia, K. W. Chew, V. Karthik, H. Selvarangaraj, P. Selvakumar, P. Sivashanmugam and P. L. Show, *Energy*, 2022, **244**, 122604.

8 K. Velusamy, J. B. Isabel, S. Periyasamy, A. Thiruvenkadam, H. Ravikumar, S. K. Gupta and E. A. López-Maldonado, *J. Taiwan Inst. Chem. Eng.*, 2024, 105732.

9 M. T. Nazari, J. Mazutti, L. G. Basso, L. M. Colla and L. Brandli, *Environ. Dev. Sustain*, 2021, **23**, 11139–11156.

10 D. T. Oyekunle, E. A. Gendy, M. Barasa, D. O. Oyekunle, B. Oni and S. K. Tiong, *Clean. Eng. Technol.*, 2024, **21**, 100773.

11 N. Rodoshi Khan and A. Bin Rashid, *Energy Convers. Manage.: X*, 2024, **22**, 100590.

12 G. M. Mathew, D. Raina, V. Narisetty, V. Kumar, S. Saran, A. Pugazhendi, R. Sindhu, A. Pandey and P. Binod, *Sci. Total Environ.*, 2021, **794**, 148751.

13 M. P. Duarte, A. Hamilton and R. Naccache, in *Biomass to Bioenergy: Modern Technological Strategies for Biorefineries*, Woodhead Publishing, 2024, pp. 73–108.

14 R. Nayab, M. Imran, M. Ramzan, M. Tariq, M. B. Taj, M. N. Akhtar and H. M. N. Iqbal, *Fuel*, 2022, **328**, 125254.

15 S. Hasannia, M. Kazemeini and A. Seif, *Energy Convers. Manage.*, 2024, **303**, 118201.

16 V. G. Nguyen, P. Sharma, M. Dzida, V. H. Bui, H. S. Le, A. S. El-Shafay, H. C. Le, D. T. N. Le and V. D. Tran, *Energy Fuels*, 2024, **38**, 2654–2689.

17 Y. Zhao, C. Wang, L. Zhang, Y. Chang and Y. Hao, *Renewable Sustainable Energy Rev.*, 2021, **140**, 110661.

18 B. Karmakar and G. Halder, *Energy Convers. Manage.*, 2019, **182**, 307–339.

19 A. G. Alsultan, N. Asikin-Mijan, Z. Ibrahim, R. Yunus, S. Z. Razali, N. Mansir, A. Islam, S. Seenivasagam and Y. H. Taufiq-Yap, *Catalysts*, 2021, **11**, 1261.

20 B. Changmai, C. Vanlalveni, A. P. Ingle and R. Bhagat, *RSC Adv.*, 2020, **10**, 41625.

21 I. M. R. Fattah, H. C. Ong, T. M. I. Mahlia, M. Mofijur, A. S. Silitonga, S. M. A. Rahman and A. Ahmad, *Front. Energy Res.*, 2020, **8**, 1–17.

22 A. Mukhtar, S. Saqib, H. Lin, M. Ul, H. Shah, S. Ullah, M. Younas, M. Rezakazemi, M. Ibrahim, A. Mahmood, S. Asif and A. Bokhari, *Renewable Sustainable Energy Rev.*, 2021, **157**, 112012.

23 Z. Zailan, M. Tahir, M. Jusoh and Z. Y. Zakaria, *Renewable Energy*, 2021, **175**, 430–452.

24 C. C. Chong, Y. W. Cheng, M. K. Lam, H. D. Setiabudi and D.-V. N. Vo, *Energy Technol.*, 2021, **9**, 2100303.

25 T. Parangi and M. K. Mishra, *Comments Inorg. Chem.*, 2020, **40**, 176–216.

26 X. Tan, P. Sudarsanam, J. Tan, A. Wang, H. Zhang, H. Li and S. Yang, *J. Environ. Chem. Eng.*, 2021, **9**, 104719.

27 M. Zhang, A. Sun, Y. Meng, L. Wang, H. Jiang and G. Li, *Microporous Mesoporous Mater.*, 2015, **204**, 210–217.

28 B. Karmakar, B. Ghosh and G. Halder, *Front. Energy Res.*, 2020, **8**, 576792.

29 G. Yadav and M. Ahmaruzzaman, *ACS Omega*, 2022, **7**, 28534–28544.

30 J. V. L. Ruatpuia, B. Changmai, A. Pathak, L. A. Alghamdi, T. Kress, G. Halder, A. E. H. Wheatley and S. L. Rokhum, *Renewable Energy*, 2023, **206**, 597–608.

31 A. Hamilton, M. Pains Duarte and R. Naccache, *Part. Part. Syst. Charact.*, 2024, **42**, 2400147.

32 J. M. Fonseca, L. Spessato, A. L. Cazetta, C. da Silva and V. de C. Almeida, *Chem. Eng. Process.*, 2022, **170**, 108668.

33 A. Takagaki, M. Toda, M. Okamura, J. N. Kondo, S. Hayashi, K. Domen and M. Hara, *Catal. Today*, 2006, **116**, 157–161.

34 I. F. Nata, M. D. Putra, C. Irawan and C. K. Lee, *J. Environ. Chem. Eng.*, 2017, **5**, 2171–2175.

35 F. A. Dawodu, O. Ayodele, J. Xin, S. Zhang and D. Yan, *Appl. Energy*, 2014, **114**, 819–826.

36 M. Toda, A. Takagaki, M. Okamura, J. N. Kondo, S. Hayashi, K. Domen and M. Hara, *Nature*, 2005, **438**(7065), 178.

37 L. Tumkot, A. T. Quitain, P. Boonnoun, N. Laosiripojana, T. Kida and A. Shotipruk, *ACS Omega*, 2020, **5**, 23542–23548.

38 W. Y. Lou, M. H. Zong and Z. Q. Duan, *Bioresour. Technol.*, 2008, **99**, 8752–8758.

39 M. H. Zong, Z. Q. Duan, W. Y. Lou, T. J. Smith and H. Wu, *Green Chem.*, 2007, **9**, 434–443.

40 M. Okamura, A. Takagaki, M. Toda, J. N. Kondo, K. Domen, T. Tatsumi, M. Hara and S. Hayashi, *Chem. Mater.*, 2006, **18**, 3039–3045.

41 M. Sevilla and A. B. Fuertes, *Carbon*, 2009, **47**, 2281–2289.

42 H. Simsir, N. Eltugral and S. Karagoz, *Bioresour. Technol.*, 2017, **246**, 82–87.

43 M. Sevilla and A. B. Fuertes, *Chem. – Eur. J.*, 2009, **15**, 4195–4203.

44 L. Yu, C. Falco, J. Weber, R. J. White, J. Y. Howe and M. M. Titirici, *Langmuir*, 2012, **28**, 12373–12383.

45 N. Sahiner, *Int. J. Hydrogen Energy*, 2018, **43**, 9687–9695.

46 M. Zhang, H. Yang, Y. Liu, X. Sun, D. Zhang and D. Xue, *Carbon*, 2012, **50**, 2155–2161.

47 C. Falco, N. Baccile and M. M. Titirici, *Green Chem.*, 2011, **13**, 3273–3281.

48 M. M. Titirici, M. Antonietti and N. Baccile, *Green Chem.*, 2008, **10**, 1204–1212.

49 P. Liu, W. Cai, J. Wei, Z. Cai, M. Zhu, B. Han, Z. Yang, J. Chen and M. Jaroniec, *J. Mater. Chem. A*, 2019, **7**, 18840–18845.

50 J. Su, C. Fang, M. Yang, Y. Cheng, Z. Wang, Z. Huang and C. You, *J. Mater. Sci. Technol.*, 2020, **38**, 183–188.

51 T. V. De Medeiros, J. Manioudakis, F. Noun, J. R. Macairan, F. Victoria and R. Naccache, *J. Mater. Chem. C*, 2019, **7**, 7175–7195.

52 Y. Gao, J. Remón and A. S. Matharu, *Green Chem.*, 2021, **23**, 3502–3525.

53 A. P. da Luz Corrêa, P. M. M. da Silva, M. A. Gonçalves, R. R. C. Bastos, G. N. da Rocha Filho and L. R. V. da Conceição, *Arabian J. Chem.*, 2023, **16**, 104964.

54 D. Lee, *Molecules*, 2013, **18**, 8168–8180.

55 M. Tariq, S. Ali, F. Ahmad, M. Ahmad, M. Zafar, N. Khalid and M. A. Khan, *Fuel Process. Technol.*, 2011, **92**, 336–341.

56 L. J. Konwar, P. Mäki-Arvela and J. P. Mikkola, *Chem. Rev.*, 2019, **119**, 11576–11630.

57 Z. Zhou, X. Zhang, F. Yang and S. Zhang, *J. Cleaner Prod.*, 2019, **215**, 13–21.

58 S. Zhang, H. Pan, J. Huang, Y. Li and H. Zhang, *Front. Chem.*, 2022, **10**, 882235.

59 Y. Wang, D. Wang, M. Tan, B. Jiang, J. Zheng, N. Tsubaki and M. Wu, *ACS Appl. Mater. Interfaces*, 2015, **7**, 26767–26775.

60 S. Niu, Y. Ning, C. Lu, K. Han, H. Yu and Y. Zhou, *Energy Convers. Manage.*, 2018, **163**, 59–65.

61 Z. E. Tang, S. Lim, Y. L. Pang, S. H. Shuit and H. C. Ong, *Renewable Energy*, 2020, **158**, 91–102.

62 F. C. P. Ribeiro, J. L. Santos, R. O. Araujo, V. O. Santos, J. S. Chaar, J. A. S. Tenório and L. K. C. de Souza, *Renewable Energy*, 2024, **220**, 119653.

63 N. Abdulwali, J. van der Zalm, A. R. Thiruppathi, A. Khaleel and A. Chen, *Appl. Surf. Sci.*, 2024, **642**, 158579.

64 Y. Qi, M. Zhang, L. Qi and Y. Qi, *RSC Adv.*, 2016, **6**, 20814–20823.

65 W. Zhang, H. Tao, B. Zhang, J. Ren, G. Lu and Y. Wang, *Carbon*, 2011, **49**, 1811–1820.

66 M. Yang, J. Su, C. Fang, Y. Cheng, Y. Li, Y. Yan and W. Lei, *Mol.*, 2023, **28**, 5756.

67 A. P. da L. Corrêa, R. R. C. Bastos, G. N. da R. Filho, J. R. Zamian and L. R. V. da Conceição, *RSC Adv.*, 2020, **10**, 20245.

68 A. S. Yusuff, K. A. Thompson-Yusuff and J. Porwal, *RSC Adv.*, 2022, **12**, 10237–10248.

69 H. S. El Saey, A. O. Abo EL Naga, M. El Saied, S. A. Shaban, S. A. Abdel-Gawad and S. A. Salih, *Biomass Bioenergy*, 2023, **176**, 106892.

70 M. Cao, L. Peng, Q. Xie, K. Xing, M. Lu and J. Ji, *Bioresour. Technol.*, 2021, **324**, 124614.

71 G. Wen, D. Na, Y. Yan and H. Liu, *New J. Chem.*, 2024, **48**, 18796.

72 S. Jing, S. Shen, X. Peng, H. Pan, C. Wang, B. Wu, J. Li, T. Wu and Y. Xing, *Fuel Process. Technol.*, 2021, **224**, 107004.

73 P. A. Russo, M. M. Antunes, P. Neves, P. V. Wiper, E. Fazio, F. Neri, F. Barreca, L. Mafra, M. Pillinger, N. Pinna and A. A. Valente, *J. Mater. Chem. A*, 2014, **2**, 11813–11824.

74 K. Nakajima and M. Hara, *ACS Catal.*, 2012, **2**, 1296–1304.

75 H. Zhang, X. Luo, K. Shi, T. Wu, F. He, H. Yang, S. Zhang and C. Peng, *Carbon*, 2019, **147**, 134–145.

76 S. Chozhavendhan, M. V. P. Singh, B. Fransila, R. P. Kumar and G. K. Devi, *Curr. Res. Green Sustainable Chem.*, 2020, **1–2**, 1–6.

77 A. Bohlouli and L. Mahdavian, *Biofuels*, 2021, **12**, 885–898.

78 P. Verma and M. P. Sharma, *Renewable Sustainable Energy Rev.*, 2016, **62**, 1063–1071.

79 O. D. Okechukwu, E. Joseph, U. C. Nonso and N.-O. Kenechi, *Clean. Chem. Eng.*, 2022, **3**, 100038.

80 B. Zheng, L. Chen, L. He, H. Wang, H. Li, H. Zhang and S. Yang, *Ind. Crops Prod.*, 2024, **210**, 118058.

81 C. M. Mendaros, A. W. Go, W. J. T. Nietes, B. E. J. O. Gollem and L. K. Cabatingan, *Renewable Energy*, 2020, **152**, 320–330.

82 M. Aliyu, B. R. Moser, F. A. Alharthi and U. Rashid, *Process Saf. Environ. Prot.*, 2024, **187**, 1126–1139.

83 S. F. Ibrahim, N. Asikin-Mijan, M. L. Ibrahim, G. Abdulkareem-Alsultan, S. M. Izham and Y. H. Taufiq-Yap, *Energy Convers. Manage.*, 2020, **210**, 112698.

84 B. Zhang, J. Ren, X. Liu, Y. Guo, Y. Guo, G. Lu and Y. Wang, *Catal. Commun.*, 2010, **11**, 629–632.

This journal is © The Royal Society of Chemistry 2025

Catal. Sci. Technol., 2025, **15**, 6499–6512 | **6511**

85 R. O. Araujo, V. O. Santos, F. C. P. Ribeiro, J. da S. Chaar, A. M. Pereira, N. P. S. Falcão and L. K. C. de Souza, *Energy Convers. Manage.*, 2021, **228**, 113636.

86 B. Zhang, M. Gao, J. Geng, Y. Cheng, X. Wang, C. Wu, Q. Wang, S. Liu and S. M. Cheung, *Renewable Energy*, 2021, **164**, 824–832.

87 S. L. Rokhum, B. Changmai, T. Kress and A. E. H. Wheatley, *Renewable Energy*, 2022, **184**, 908–919.

88 Z. Hussain and R. Kumar, *Mater. Today: Proc.*, 2018, **5**, 18287–18296.

89 M. Athar and S. Zaidi, *J. Environ. Chem. Eng.*, 2020, **8**, 104523.

90 E. G. Al-Sakkari, O. M. Abdeldayem, S. T. El-Sheltawy, M. F. Abadir, A. Soliman, E. R. Rene and I. Ismail, *Fuel*, 2020, **279**, 118519.

91 N. Ghosh, D. Rhithuparna, R. Khatoon, S. L. Rokhum and G. Halder, *J. Cleaner Prod.*, 2023, **394**, 136362.

92 X. Mo, D. E. López, K. Suwannakarn, Y. Liu, E. Lotero, J. G. Goodwin and C. Lu, *J. Catal.*, 2008, **254**, 332–338.

93 Y. Pi, W. Liu, J. Wang, G. Peng, D. Jiang, R. Guo and D. Yin, *Front. Chem.*, 2022, **10**, 944398.

94 E. Calcio Gaudino, G. Cravotto, M. Manzoli and S. Tabasso, *Green Chem.*, 2019, **21**, 1202–1235.

6512 | *Catal. Sci. Technol.*, 2025, **15**, 6499–6512

This journal is © The Royal Society of Chemistry 2025